TSOUCARIS, G. (1970). *Acta Cryst.* A**26**, 492-499.
VAN DEN HARK, TH. E. M., PRICK, P. A. J. & BEURSKENS, P. T. (1976). *Acta Cryst.* A**32**, 816-821.
WANG, B. C. (1985). In *Methods of Enzymology*, Vol. 115: *Diffraction Methods for Biological Macromolecules*, edited by H. WYCKOFF, C. H. W. HIRS & S. N. TIMASHEFF. New York: Academic Press.
WEISS, G. H., SHMUELI, U., KIEFER, J. E. & WILSON, A. J. C. (1985). *Structure and Statistics in Crystallography*, edited by A. J. C. WILSON, pp. 23-42. Guilderland: Adenine Press.
WIENER, N. (1949). *Extrapolation, Interpolation, and Smoothing of Stationary Time Series.* Cambridge, MA: MIT Press.
WILKINS, S. W. & STUART, D. (1986). *Acta Cryst.* A**42**, 197-202.
WILSON, A. J. C. (1949). *Acta Cryst.* **2**, 318-321.
WILSON, A. J. C. (1952). *Research*, **5**, 589-590.
WILSON, A. J. C. (1964). *Acta Cryst.* **17**, 1591-1592.
WILSON, A. J. C. (1987). *Acta Cryst.* A**43**, 554-556.
WILSON, I. A., SKEHEL, J. J. & WILEY, D. C. (1981). *Nature (London)*, **289**, 366-373.

Acta Cryst. (1988). A**44**, 545-551

Low-Resolution Phase Extension and Refinement by Maximum Entropy

BY A. D. PODJARNY AND D. MORAS

Laboratoire de Cristallographie Biologique, IBMC, 15 Rue R. Descartes, 67084 Strasbourg, France

J. NAVAZA

Laboratoire de Physique, Centre Universitaire Pharmaceutique, Tour B, 92290 Châtenay-Malabry, France

AND P. M. ALZARI

Immunologie Structurale, Institut Pasteur, 25 Rue du Dr Roux, 75724 Paris, France

(*Received* 27 *October* 1987; *accepted* 11 *March* 1988)

Abstract

The problem of phase refinement and extension at very low resolution (30-25 Å) is treated with an algorithm that combines a maximum-entropy approach, a binary modelling of the electron density, refinement of the proposed map against the observed amplitudes and solvent flattening outside a molecular envelope. The algorithm is applied to data for the complex of aspartyl-tRNA and aspartyl-tRNA synthetase in three different cases: (1) X-ray amplitudes and phases calculated from a partial model; (2) mixed observed and calculated X-ray amplitudes and phases from a partial model; and (3) observed neutron amplitudes and phases from a very approximate model. The change of correlation with the correct map at 30 Å resolution is used as a measure of correctness. Upon application of the algorithm, this correlation changes from 59 to 97% in case 1, from 59 to 77% in case 2 and from 72 to 90% in case 3. In all cases, the method is successful in correcting large phase errors, deleting noise regions and producing the correct low-resolution molecular image.

Introduction

Macromolecular crystallography is a unique tool for imaging the structures of protein and nucleic acids. Images are obtained from the Fourier transform of the diffraction pattern of the crystal. In the classical picture the scattered radiation consists of X-rays at a resolution where individual atoms are close to being resolved, and the phases with their error estimation are obtained by the multiple-isomorphous-replacement (MIR) method (Blow & Crick, 1959).

When all the necessary conditions are fulfilled, the classical approach is extremely powerful and a very detailed image of the macromolecule is obtained. However, it is not always possible to obtain high-quality crystals that diffract to high resolution and the necessary heavy-atom derivatives. In this case, alternative phasing techniques can be used. These are varied, and the following examples can be cited (the list is clearly not exhaustive).

(1) Electron microscopy of an ordered specimen can give a 3D image of 7 Å resolution (Henderson & Unwin, 1975), though most of the image reconstructions have been limited to about 25 Å resolution.

(2) A low-resolution translation search with a crude model can generate phases between 30 and 15 Å resolution (Podjarny *et al.*, 1987).

(3) Neutron diffraction with different D_2O/H_2O levels can be used instead of heavy atoms, if one component is known. Phases are generally good to 30 Å resolution, and can extend as far as 15 Å resolution (Bentley, Lewitt-Bentley, Finch, Podjarny & Roth, 1984).

0108-7673/88/040545-07$03.00

(4) If the structure of a highly homologous molecule is known, molecular replacement methods can be used to derive high-resolution (1·5–3 Å) phases (Rossmann, 1972).

(5) If the molecular packing includes non-crystallographic symmetry, averaging of independent units can be used to improve and/or extend phase information (Rossmann & Blow, 1963).

(6) If the crystal includes a large volume of solvent and some MIR information is known, solvent-flattening techniques can be used to improve and/or extend phase information to high resolution (Hendrickson, Klippenstein & Ward, 1975).

This paper is concerned with cases 1–3 where there is only some low-resolution phase information. This case was not relevant to the first applications of macromolecular crystallography, since attention was focused on small closely packed proteins and there were very few reflections at a resolution of 30 Å. However, as larger and more complex systems are studied, low-resolution scattering becomes important in obtaining the molecular image.

The case of the aspartyl-tRNA synthetase complex from yeast

As a test case where the correct determination of 30 Å resolution phases is important, the complex of aspartyl-tRNA and aspartyl-tRNA synthetase was chosen. The complex involves a dimer of aspartyl-tRNA synthetase ($M_r = 125\,000$) and two aspartyl-tRNA molecules ($M_r = 24\,160$). It crystallizes in space group $I432$ ($a = 354$ Å) with a diffraction pattern extending to 7·9 Å resolution (Lorber, Giegé, Ebel, Berthet, Thierry & Moras, 1983), and in space group $P2_12_12_1$ ($a = 220$, $b = 145$, $c = 85$ Å), with a diffraction pattern extending to 2·7 Å resolution (Ruff, Mikol, Lorber, Cavarelli, Mitschler, Giegé, Thierry & Moras, 1987).

At present, native and heavy-atom data are available for the cubic form, as well as enough crystals of the orthorhombic form to collect a full data set. However, for historical and technical reasons the only complete diffraction data available during a long period was the native diffraction of the cubic form. Therefore, considerable effort was devoted to the *ab initio* phasing of the native cubic intensities, which produced a 15 Å model consisting of 140 Gaussian scattering centers, 70 for the synthetase dimer and 70 for the two tRNA molecules (Podjarny *et al.*, 1987). Two different data sets were used to obtain this model: (1) X-ray diffraction amplitudes extending to 7·9 Å resolution but lacking 41 very-low-resolution reflections (4629 reflections, of which 1669 were used in the refinement); and (2) neutron diffraction amplitudes to 18 Å resolution, including 28 of the 41 missing X-ray reflections (370 reflections, of which 177 were used in the refinements).

The phasing effort proceeded stepwise in resolution. A rough low-resolution model was first obtained using translation functions with Gaussian spheres, and then painstakingly improved through alternate cycles of density modification (to impose real-space constraints), difference maps and least-squares refinement (to obtain the best agreement between model and observed amplitudes). During this effort, it became clear that an alternative and more automatic way to refine and extend low-resolution phases was necessary if the method was to become general. This alternative method should have both the power of density modification to impose real space constraints and of least-squares refinements to maximize the agreement of model and observed amplitudes, and is proposed below.

Theoretical outline

Information theory has provided a strong conceptual framework in connection with electron density reconstruction (Collins, 1982; Wilkins, Varghese & Lehmann, 1983; Bricogne, 1984; Livesey & Skilling, 1985; Navaza, 1985). In particular, the method proposed in this paper simultaneously imposes a real-space modelling and the agreement of observed and calculated amplitudes. Different models are possible, depending on the resolution range of interest. For example, it was shown (de Rango & Navaza, 1984; Navaza, 1986) that it is possible to obtain a map of quality comparable to a 1–1·5 Å calculated map starting from a 3·6–3 Å phase set and imposing a model of Gaussian spheres. Alternatively, for low resolution it was found (Cannillo, Oberti & Ungaretti, 1983) that a binary representation where the map density is constrained to take one of two possible values is adequate. The present formalism can be used to produce a binary density map of limited Fourier spectrum by fitting the data under artificially severe constraints.

We briefly recall the fundamental results of the theory developed by Navaza (1985), to which the reader is referred for details. The maximum-entropy estimate of the electron density function $\langle m \rangle$ is the average value over the set A of all admissible maps m, given by

$$\langle m(r) \rangle = \int_A P_{\mathrm{me}}(m) m(r) \mathbf{D}m \qquad (1)$$

where the probability distribution $P_{\mathrm{me}}(m)$ is the solution of the constrained maximization of the entropy functional

$$H(P) = -\int_A P(m) \ln [P(m)] \mathbf{D}m. \qquad (2)$$

Under very general conditions $\langle m \rangle$ is a functional of the Lagrange multipliers associated with the experimental information (diffraction data and possibly available phases). The actual functional form is

determined by the information that defines the domain of admissible maps (positivity, molecular envelope, upper map limit).

In this paper the information used was

$$\rho_{\min}(r) < m(r) < \rho_{\max}(r) \qquad (3a)$$

$$\langle F(h)\rangle = (1/V)\int \langle m(r)\rangle \exp(2\pi i h r)\, dr^3 = F_{\text{obs}}(h), \qquad h \in \mathbf{H} \qquad (3b)$$

$$|\langle F(k)\rangle| = |(1/V)\int \langle m(r)\rangle \exp(2\pi i k r)\, dr^3| = |F_{\text{obs}}(k)|, \qquad k \in \mathbf{K} \qquad (3c)$$

where **H** is the set of Miller indices of the structure factors of known amplitude and phase, **K** is the set of Miller indices of the structure factors of known amplitude and unknown phase, and $\rho_{\min}$ and $\rho_{\max}$ are the minimum and maximum allowed density values.

This information leads to the maximum entropy estimate $\langle m\rangle$ given by

$$\langle m(r)\rangle = 0{\cdot}5(\rho_{\max}+\rho_{\min}) + 0{\cdot}5\,\delta\rho\{1/[\chi(r)\delta\rho] - 1/\tanh[\chi(r)\delta\rho]\} \qquad (4)$$

with

$$\delta\rho = 0{\cdot}5(\rho_{\max}-\rho_{\min})$$

and

$$\chi(r) = \sum_{b\in\mathbf{H}\cup\mathbf{K}} \lambda(b)\exp(-2\pi i b r). \qquad (5)$$

All estimates are thus functions of the set of Lagrange multipliers which satisfy the system of equations (3*b*), (3*c*) and

$$\lambda(k)^*\langle F(k)\rangle - \lambda(k)\langle F(k)\rangle^* = 0, \qquad k \in \mathbf{K}. \qquad (6)$$

In particular, the predicted values of the Fourier coefficients F_{ent} are obtained in modulus and phase from the Fourier transform of $\langle m(r)\rangle$.

For unrealistically small values of $\rho_{\max}$, no map will simultaneously satisfy the constraints (3), and the Lagrange multipliers will diverge. Equations (4) and (5) imply that, for large enough values of the Lagrange multipliers, $\langle m\rangle$ will tend to $\rho_{\min}$ or $\rho_{\max}$. Therefore, the binary modelling can be obtained by artificially reducing the upper density limit of the admissible maps.

Numerical algorithm

The algorithm flow chart is represented in Fig. 1. The first part (top half of the chart) produces an initial set of Lagrange multipliers λ at resolution Resin, the parameters $\rho_{\max}$ and $F(000)$, and optionally a molecular envelope (Mask). It starts from the observed structure factors F_{obs} known in modulus and phase at the same resolution Resin (if a figure of merit w is available for the input phases, the input amplitudes are taken as $w|F_{\text{obs}}|$).

Program *D* calculates an input map, and produces a value of $\rho_{\min}$ and an artificially low value of $\rho_{\max}$. It estimates $F(000)$ by imposing a pre-assigned ratio $(\rho_{\max}/\rho_{\min})$ and calculates a molecular envelope by a procedure originally developed by Westbrook (1985). The λ's associated with this information are calculated by the program *P*1, as described by Navaza (1985).

The second part (bottom half of the chart) constitutes the core of the algorithm. Starting from a set of λ's at resolution Resin and the observed amplitudes $|F_{\text{obs}}|$ at resolution Resout, the program *P*2 gives new λ's and estimated phases of the structure factors at resolution Resout. Optionally, the molecular envelope and the input parameters $F(000)$ and $\rho_{\max}$ may be updated.

This central part of the algorithm can be used either for phase refinement (Resout = Resin) or iteratively for phase extension and refinement (Resout > Resin), in which case Resout can be reached from Resin in one or several steps. The only difference between *P*1 and *P*2 is that while in the first case (phases and moduli given as input information) the problem has a unique solution, in the second case (only moduli given) the resulting λ's depend to some extent on their initial values.

Results

The algorithm described above was used to improve the phases at 30 Å resolution of the tRNA synthetase

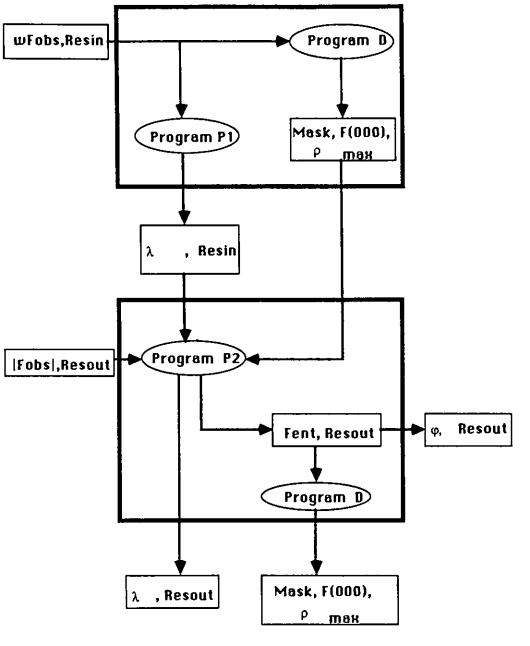

Fig. 1. Flow chart of the proposed algorithm. The large box at the top represents the first part, the large box at the bottom the second part. Data to the left are input data, data to the right are output data. For a detailed explanation, see text.

Table 1. *Comparisons between pairs of test cases*

	Resolution (Å)	Number of reflections	$\langle\delta\varphi\rangle$ (°)	R.m.s. $(w\delta\varphi)$ (°)	WM	R factor	R_{sq} factor	F correlation
1 (*a*) F_{cal}, φ_{cal} (*b*) F_{part}, φ_{part}	30	110	44·5	75·8	0·623	0·53	0·58	0·64
2 (*a*) F_{cal}, φ_{cal} (*b*) F_{ent}, φ_{ent} starting from phases (1*b*)	30	110	33·2	67·3	0·70	0·34	0·44	0·87
3 (*a*) F_{cal}, φ_{cal} (*b*) F_{ent}, φ_{ent} starting from phases (1*b*)	25	179	45·8	69·4	0·68	0·35	0·44	0·88
4 (*a*) F_{cal}, φ_{cal} (*b*) F_{part}, φ_{part} omitting reflections with $w<0·01$	30	99	40·7	52·8	0·80	0·49	0·5	0·71
5 (*a*) F_{cal}, φ_{cal} (*b*) F_{ent}, φ_{ent} starting from phases (4*b*)	30	110	12·5	10·5	0·99	0·30	0·32	0·98
6 (*a*) F_{cal}, φ_{cal} (*b*) F_{ent}, φ_{ent} starting from phases (4*b*)	25	179	28·9	19·3	0·97	0·32	0·33	0·97
7 (*a*) F_{obs}, φ_{cal} (*b*) F_{part}, φ_{part}	30	110	44·5	78·2	0·60	0·59	0·60	0·61
8 (*a*) F_{obs}, φ_{cal} (*b*) F_{ent}, φ_{ent} starting from phases (7*b*)	30	110	54·9	54·8	0·79	0·31	0·37	0·89
9 (*a*) F_{neu}, φ_{cal} (*b*) F_{mod}, φ_{mod}	30	103	61·9	63·7	0·72	0·32	0·26	0·95
10 (*a*) F_{neu}, φ_{cal} (*b*) F_{ent}, φ_{ent} with individual check of largest centrosymmetric reflections	30	103	58·4	36·6	0·89	0·33	0·35	0·94
11 (*a*) F_{neu}, φ_{cal} (*b*) F_{ent}, φ_{ent} starting from phases (10*b*)	25	167	74·1	42·5	0·86	0·32	0·35	0·94

Notes: F, φ stands for the structure factor $|F|e^{i\varphi}$; $\delta\varphi=\varphi(a)-\varphi(b)$; w = figure of merit. F correlation $=[\sum|F(a)||F(b)|]/\{[\sum(|F(a)|)^2][\sum(|F(b)|)^2]\}^{1/2}$. WM $=\{\sum[|F(a)|^2\cos(\delta\varphi)]\}/[\sum|F(a)|^2]$. In lines 7 and 8, the $|F_{obs}|$ set is combined (see text).

complex (Podjarny *et al.*, 1987), used as a test case. Three different cases were treated.

(1) *Calculated amplitudes from complete model and phases from partial model*

As a first test, a fully calculated case was studied. A model of the complex composed of 140 spheres, 70 corresponding to the tRNA and 70 corresponding to the synthetase, was refined at 30 Å against neutron data; one tRNA molecule which was particularly well positioned represented after refinement 42·2% of the scattering power (Podjarny *et al.*, 1987). This complete model was taken as the correct one, and used to calculate structure factors $|F_{cal}|\exp(i\varphi_{cal})$. A partial model was built without this tRNA molecule, and used for the calculation of the input test phases, φ_{part}, as well as for the corresponding amplitudes, $|F_{part}|$. This introduced a systematic phase error which changed the phases of very intense centrosymmetric reflections and corresponded to a low correlation value WM (0·64) between the maps phased with correct and partial phases (see line 1 of Table 1).

The structure-factor amplitudes from the complete model ($|F_{cal}|$) and the partial model ($|F_{part}|$) were used to calculate a Sim weight, Wsim. Phases were refined to 30 Å and extended to 25 Å. The starting map (Fig. 2*b*) was calculated with 30 Å phases from the partial model φ_{part} and amplitudes Wsim $|F_{cal}|$. The comparison of final phases, φ_{ent}, with the correct phases, φ_{cal}, is shown in Table 1, lines 2 and 3. An electron density map calculated with these phases (Fig. 2*c*) shows that the omitted tRNA was correctly represented when compared with the complete model (Fig. 2*a*). However, a few large reflections with wrong phases were not corrected by the algorithm.

Consequently, Sim weights were recalculated for the partial phases, adding an extra constraint. The r.m.s. standard deviation, r.m.s.$(\delta F)=[\langle(|F_{part}|-|F_{cal}|)^2\rangle]^{1/2}$ was calculated over the whole data set, and Wsim was set to zero if abs $(|F_{part}|-|F_{cal}|)>3$r.m.s.(δF), deleting two extra reflections from the data set. After deleting these reflections, the phase error was improved (see Table 1, line 4).

The algorithm was applied with these new weights, starting from φ_{part} and Wsim$|F_{cal}|$. Phases were refined at 30 Å and extended to 25 Å resolution. The comparison of the refined phases and the correct ones is shown in Table 1, line 5, and the map calculated with the refined phases to 30 Å is shown in Fig. 2(*d*). This map is practically identical to the correct one. The two reflections which had been omitted were predicted with the correct phase. The result of the phase extension to 25 Å is shown in Table 1, line 6. It should

be noted that in this case also the high correlation (0·968) shows that the 25 Å map is very close to the correct one.

(2) *Observed and calculated amplitudes from complete model and calculated phases from partial model*

As a continuation, the test described above was repeated with observed X-ray amplitudes and the same model refined against X-ray data. The complete model was used to calculate $|F_{cal}|$ and φ_{cal}. Since the X-ray amplitudes of 41 very-low-resolution reflections were not observed, they were replaced by the calculated values. Therefore, the amplitude set $|F_{obs}|$ was a mixed set, with 69 observed and 41 calculated reflections. The partial model was used to calculate $|F_{part}|$ and φ_{part}, whose comparison with $|F_{obs}|$ and φ_{cal} is shown in line 7 of Table 1. Fig. 3(*b*) shows a map calculated from $2|F_{obs}|-|F_{part}|$ and φ_{part}, and Fig. 3(*a*) shows the correct map calculated from $|F_{obs}|$ and φ_{cal}. It is clear that the error in the partial phases creates a very large noise region, mostly responsible for the low value of WM.

Upon application of the algorithm as described above for phase refinement at 30 Å, new phases φ_{ent} were calculated. The comparison with φ_{cal} is shown in line 8 of Table 1. Note the improvement of WM from 0·56 to 0·79. Fig. 3(*c*) shows the map as calculated with $|F_{obs}|$ and φ_{ent}, indicating that the noise region is clearly diminished.

(3) *Observed amplitudes and poor phases*

As a third test, the initial data set consisted of observed neutron amplitudes $|F_{neu}|$ and phases φ_{mod} from a model of five Gaussian spheres. The interest of this case is that the model was derived from *ab initio* translation searches with spheres and refined against neutron amplitudes in the very early stages of solution of the structure, and that improvement of the corresponding phase set, obtained painstakingly with several stages of refinement and density modification, was crucial for obtaining the final solution (Podjarny *et al.*, 1987).

A 'correct' phase set, φ_{cal}, was obtained from the last model refined against neutron amplitudes. Measured against this set, the quality of the φ_{mod} phases was poor, as shown in Table 1, line 9. This is due to the presence of large centrosymmetric reflections with wrong phases. The execution of the algorithm failed to correct these wrong phases, starting either from the complete data set or a weighted

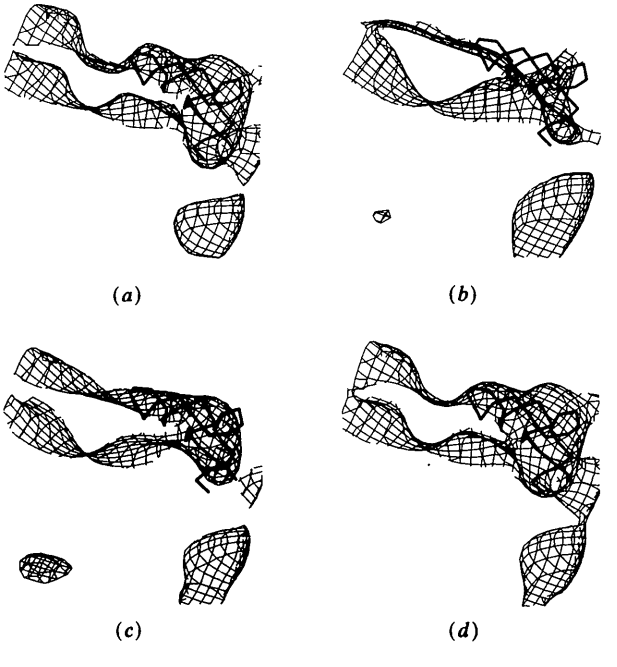

Fig. 2. (*a*) Superposition of a tRNA backbone (to be omitted in the partial model) and an electron density map calculated from complete model data at 30 Å resolution. (*b*) Same as (*a*), with an electron density map with correct weighted amplitudes (Wsim $|F_{cal}|$) and phases from partial model (φ_{part}). (*c*) Same as (*a*), with an electron density map with correct amplitudes ($|F_{cal}|$) and phases from entropy algorithm without cutoff on Sim weighting (φ_{ent}). Correlation with correct map = 0·71. (*d*) Same as (*c*), but including a cutoff on Sim weighting. Correlation with correct map = 0·989. Note the absence of spurious peaks.

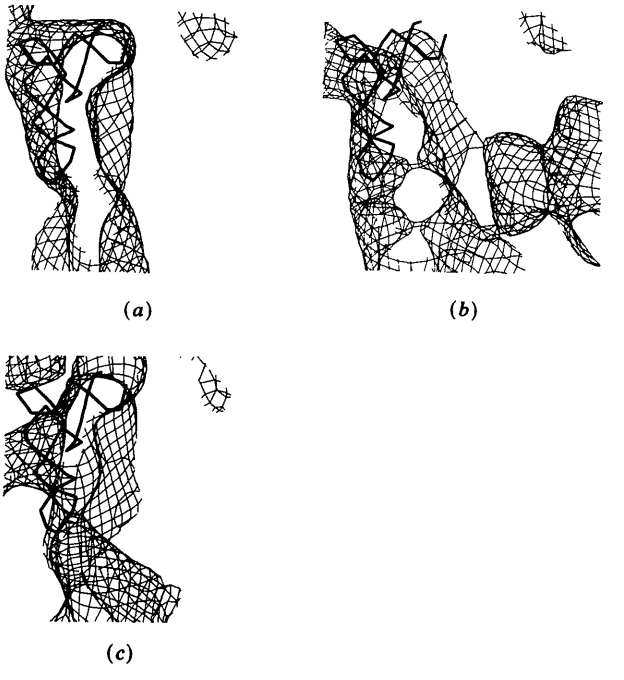

Fig. 3. (*a*) Superposition of tRNA model and correct electron density map calculated from mixed X-ray and model amplitudes $|F_{obs}|$ and model phases (φ_{cal}) at 30 Å resolution. (*b*) Same as (*a*), with electron density map calculated with amplitudes $2|F_{obs}|-|F_{cal}|$ and phases from partial model (φ_{part}). Correlation with correct map = 0·60. Note large noise regions. (*c*) Same as (*a*), with electron density map calculated with observed amplitudes $|F_{obs}|$ and refined phases (φ_{ent}). Correlation with correct map = 0·79. Note decrease of noise regions.

data set with Sim figure of merit and a r.m.s.-based cutoff.

Therefore, a different strategy was devised in which the algorithm was run separately for the prediction of each of the largest centrosymmetric reflections, starting from a data set where the corresponding phase had been omitted. This strategy succeeded in correcting the wrong phases associated with large amplitudes without introducing extra errors, that is, without changing the phases of the reflections which were originally correct. The comparison of φ_{ent} and φ_{cal} is shown in Table 1, line 10. Note that the value of the WM improved from 0·72 to 0·89. While the original map (Fig. 4*b*) had large noise regions, the final map (Fig. 4*c*) is virtually equal to the correct one (Fig. 4*a*). Phases were extended to 25 Å resolution based on the 30 Å refined phases (Table 1, line 11). Note that even with this extra resolution the value of WM is 0·76.

Concluding remarks

The tests described in this work show that the algorithm described succesfully combines the accuracy of least-squares refinement with the power of density modification to impose real-space constraints. Three different tests are described. In the first two, a systematic phase error was introduced when a large portion of the model was deleted, and in the third a very poor model was used for generating the initial phases.

With calculated data (first case), the process refined to the correct data set starting from an initial set of poor phases, and the power of correcting the noise generated from the phase error remained when using observed amplitudes (second and third cases).

In all applications it was crucial to delete from the initial phase set the reflections with erroneous phase and very large amplitudes. In the first two cases, the differences between $|F_{obs}|$ and $|F_{cal}|$ were enough to identify these reflections. In the last case these reflections were not easily identified, rendering the problem quite serious. An algorithm of systematic deletion is proposed; it is effective but lengthy. Further work on speeding up the systematic deletion is under study.

The success obtained in the refinement of a poor phase set generated *ab initio* (case 3) opens the potential for a general algorithm where phases are generated at very low resolution and extended to high resolution, using only the native amplitudes and generalized models. This will require application of this algorithm in different resolution ranges, which is currently under study.

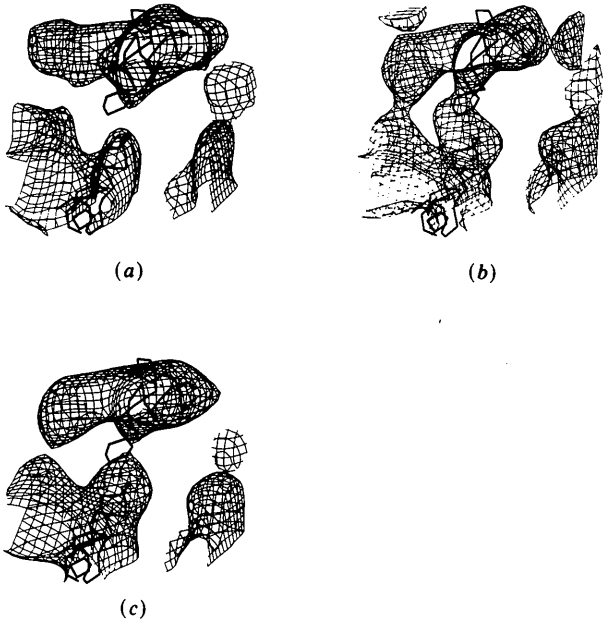

Fig. 4. (*a*) Superposition of tRNA model and correct electron density map calculated from neutron amplitudes $|F_{neu}|$ and phases from 140 spheres model data set (φ_{cal}) at 30 Å resolution. (*b*) Same as (*a*), with electron density map calculated with amplitudes $2|F_{neu}|-|F_{mod}|$ and phases from 5-spheres model (φ_{mod}) at 30 Å resolution. WM = 0·72. Note large noise regions. (*c*) Same as (*a*), with electron density map calculated with amplitudes $|F_{neu}|$ and refined phases from this algorithm (φ_{ent}) at 30 Å resolution. WM = 0·89.

This work was supported by grants from the Centre National de la Recherche Scientifique (CNRS), the Ministère de la Recherche et de la Technologie (MRT), the Université Louis Pasteur de Strasbourg, the National Institute of Health (USA, grant R01GM34942) and a NATO travel grant to DM. We thank the University of Chicago for hospitality and support during part of this research. We thank T. N. Bhat, B. Rees, Paul B. Sigler, Edwin Westbrook and M. Zwick for useful discussions during this research.

References

BENTLEY, G. A., LEWITT-BENTLEY, A., FINCH, J. T., PODJARNY, A. D. & ROTH, M. (1984). *J. Mol. Biol.* **176**, 55-75.
BLOW, D. M. & CRICK, F. H. C. (1959). *Acta Cryst.* **12**, 794-802.
BRICOGNE, G. (1984). *Acta Cryst.* A**40**, 410-445.
CANNILLO, E., OBERTI, R. & UNGARETTI, L. (1983). *Acta Cryst.* A**39**, 68-74.
COLLINS, D. M. (1982). *Nature (London)*, **298**, 49-51.
HENDERSON, R. & UNWIN, P. N. T. (1975). *Nature (London)*, **257**, 28-32.
HENDRICKSON, W. A., KLIPPENSTEIN, G. L. & WARD, K. B. (1975). *Proc. Natl Acad. Sci. USA*, **72**, 2160-2164.
LIVESEY, A. K. & SKILLING, J. (1985). *Acta Cryst.* A**41**, 113-122.
LORBER, B., GIEGÉ, R., EBEL, J. P., BERTHET, C., THIERRY, J. C. & MORAS, D. (1983). *J. Biol. Chem.* **258**, 8429-8435.
NAVAZA, J. (1985). *Acta Cryst.* A**41**, 232-244.
NAVAZA, J. (1986). *Acta Cryst.* A**42**, 212-223.
PODJARNY, A. D., REES, B., THIERRY, J. C., CAVARELLI, J., JESIOR, J. C., ROTH, M., LEWITT-BENTLEY, A., KAHN, R.,

LORBER, B., EBEL, J. P., GIEGÉ, R. & MORAS, D. (1987). *J. Biomol. Struct. Dyn.* **5**, 187-198.
RANGO, C. DE & NAVAZA, J. (1984). NATO Workshop. Future Direct Methods, Orsay, April 1984.
ROSSMANN, M. G. (1972). Editor. *The Molecular Replacement Method.* New York: Gordon & Breach.
ROSSMANN, M. G. & BLOW, D. M. (1963). *Acta Cryst.* **16**, 39-45.
RUFF, M., MIKOL, V., LORBER, B., CAVARELLI, J., MITSCHLER, A., GIEGÉ, R., THIERRY, J. C. & MORAS, D. (1987). Notes of the School on Crystal Growth of Biological Macromolecules, Bischenberg, Alsace, France, 132 pp.
WESTBROOK, E. (1985). Private communication.
WILKINS, S. W., VARGHESE, J. N. & LEHMANN, M. S. (1983). *Acta Cryst.* A**39**, 47-60.

Acta Cryst. (1988). A**44**, 551-554

Acoustical Activity of Crystals: a Comparative Study of Three Descriptions

BY K. V. BHAGWAT AND R. SUBRAMANIAN

Nuclear Physics Division, Bhabha Atomic Research Centre, Trombay, Bombay 400 085, *India*

(*Received* 8 *December* 1987; *accepted* 11 *March* 1988)

Abstract

Two apparently different descriptions of acoustical activity - one due to Portigal & Burstein [*Phys. Rev.* (1968), **170**, 673-678] based on the concept of spatial dispersion of the elastic stiffness tensor and the other based on the rotation-gradient theory due to Truesdell & Toupin [*Encyclopedia of Physics*, (1960), Vol. III/1. Berlin: Springer], Mindlin & Tiersten [*Arch. Ration. Mech. Anal.* (1962), **11**, 415-447] - are analysed on the common basis of the first-gradient theory. A relation between the tensors used for describing the acoustical activity in the two earlier descriptions is obtained.

1. Introduction

Ever since the concept of acoustical activity was introduced by Andronov (1960) and independently by Silin (1960) there has been continued interest both in its experimental observation (Pine, 1970; Joffrin, Dorner & Joffrin, 1980; Bialas & Schauer, 1982; Quan, Fang, Zhigong & Zenyi, 1987) and its theoretical characterization (Truesdell & Toupin, 1960; Mindlin & Tiersten, 1962; Portigal & Burstein, 1968; Mindlin & Toupin, 1971; Vuzhva & Lyamov, 1977; Kumarswamy & Krishnamurthy, 1980). Recently the occurrence of acoustical activity in crystals of different point-group symmetries has been examined from two apparently different points of view (Bhagwat, Wadhawan & Subramanian, 1986; Bhagwat & Subramanian, 1986) - the theory of spatial dispersion (Portigal & Burstein, 1968) and the rotation-gradient theory (Mindlin & Tiersten, 1962). Even though both viewpoints lead to the same acoustically active crystal classes, a disturbing feature remains: the tensors describing acoustical activity in the two descriptions have different symmetries and appear to be completely unrelated.

The aim of the present paper is to show that both viewpoints can be reconciled on the basis of the more general strain-gradient theory of acoustical activity where one employs the strain and its first gradient to describe the elastic deformation (Toupin, 1962; Mindlin, 1972). We also obtain a rationale for the maximum number of independent non-vanishing components of the acoustical activity tensors.

The paper is organized as follows. In § 2 we briefly recapitulate the salient features of the spatial dispersion theory of acoustical activity due to Portigal & Burstein (1968) and the rotation-gradient theory due to Truesdell & Toupin (1960) and Mindlin & Tiersten (1962). In § 3 we consider the full first-strain-gradient theory of elasticity given by Toupin (1962). Here we establish the formal equivalence of this theory with the theory of spatial dispersion. Further we show that rotation-gradient theory results from the general theory under certain additional restrictions.

2. Résumé of two viewpoints

A. *Theory of spatial dispersion*

Portigal & Burstein (1968) explained the occurrence of acoustical activity on the basis of spatial dispersion of the elastic stiffness tensor, by writing the most general form of Hooke's law as

$$\alpha_{ij}(\mathbf{r}, t) = \int d\mathbf{r}' \int_{-\infty}^{t} dt' \, C_{ijkl}(\mathbf{r}-\mathbf{r}', t-t')\varepsilon_{kl}(\mathbf{r}', t'). \quad (2.1)$$

As usual, summation over repeated indices will be implied. The stress $\boldsymbol{\sigma}$ at a point $\mathbf{r}$ at a time t is a linear superposition of strains at points $\mathbf{r}'$ at earlier instants t'. When spatial dispersion is small one may

0108-7673/88/040551-04$03.00